PAPER

Check for updates

Triangular silver nanoprism-based chemosensor for recognition of hyaluronic acid in human biofluids: a new platform for monitoring osteoarthritis treatment using smartphone-assisted digital image analysis†

Zahra Sabri,[d] Farnaz Bahavarnia,[ab] Mohammad Hasanzadeh [ID] *[c] and Nasrin Shadjou [ID] [d]

Hyaluronic acid (HA) possesses unique viscoelastic properties and low immunogenicity, making it suitable for various biomedical purposes such as viscosupplementation in osteoarthritis treatment, assistance in eye surgery, and wound regeneration. The need for its quantification in human biofluids is crucial in clinical studies. This research work presents a novel approach using paper-based and parafilm-based photochemical techniques, employing triangular silver nanoprisms (TA-AgNPrs) as optical nanoprobes for HA detection in human biofluids. The interaction between HA and TA-AgNPrs leads to a notable change in the absorption spectrum, facilitating rapid and reliable measurement with a detection limit of less than 0.5 μM to 30 mM. The developed colorimetric setups, along with the single-drop parafilm colorimetric substrate, enable fast and *on-site* HA analysis. This research marks the maiden use of TA-AgNPrs for direct, rapid and sensitive HA detection in real samples, without the need for sample pre-preparation. The use of a digital image analysis strategy enhances the simplicity, affordability, and portability of this sensor, presenting promising potential for monitoring HA levels. This new technique is poised to enable early diagnosis of diseases associated with abnormal HA levels in human biofluids, thanks to its high sensitivity and selectivity in detecting HA.

1. Introduction

The lymphatic system serves as the main anatomical location for the adaptive immune system, where antigen-presenting cells and other white blood cells travel from the body's tissues to nearby lymph nodes for immune monitoring and the production and control of cellular immune responses. Furthermore, the lymphatic system aids in fluid drainage, removing immune complexes and interstitial matrix components that break down during regular body balance and tissue damage.[1]

Specifically, the large glycosaminoglycan hyaluronan (HA, [D-glucuronic acid] β1–3-[*N*-acetyl-D-glucosamine] β1–4) undergoes rapid turnover during inflammation and is the primary target of HA in the endothelia of afferent lymphatic vessels and lymph node sinuses.[2] Moreover, HA is a common extracellular matrix component found in high concentrations in the skin, joints, and cornea. It consists of thousands of repetitive disaccharide units, resulting in millions of Daltons in the connective tissue of both vertebrates and bacterial capsules.[3]

Moreover, HA stands out as the sole non-sulfated glycosaminoglycan possessing distinctive physicochemical and biological characteristics.[4] This polymer is highly hygroscopic and has the ability to retain water molecules, thereby creating a gel-like environment.[5–7] Even in low concentrations within aqueous environments, HA and its hyaluronate salts function as a viscoelastic system.[8–11] The human body has five hyaluronidase genes and one hyaluronidase pseudogene. The hyaluronidase genes are located on chromosome 3p21.3 (Hyal1, Hyal2, and Hyal3) and chromosome 7q31.3 (Hyal4, Hyal1 pseudogene, and PH20). The multitude of charged polar groups in HA enables it to retain water molecules and engage in numerous biologically crucial polar interactions. Conversely, the regularly repeating *N*-acetyl groups promote interactions with hydrophobic regions of cell membranes and membrane proteins, which play a vital role in cell motility.[12–14] Broadly, HA is

[a] Nutrition Research Center, Tabriz University of Medical Sciences, Tabriz, Iran

[b] Food and Drug Safety Research Center, Tabriz University of Medical Sciences, Tabriz, Iran

[c] Pharmaceutical Analysis Research Center, Tabriz University of Medical Sciences, Tabriz, Iran. E-mail: hasanzadehm@tbzmed.ac.ir

[d] Department of Nanotechnology, Faculty of Chemistry, Urmia University, Urmia, Iran
† Electronic supplementary information (ESI) available. See DOI: https://doi.org/10.1039/d4ra05396f

implicated in protective and various physiological processes, encompassing wound and burn healing, tissue regeneration, cell differentiation, morphogenesis, angiogenesis, and inflammation.[15–21] Consequently, the recognition and constant monitoring of HA in human body fluids hold significance for clinicians. Traditional techniques for detecting HA concentration generally involve electrophoresis, chromatography techniques, spectrophotometric detection, and electrochemical tests, fluorescence, or mass spectrometric detection.[22–25] Despite delivering excellent detection limits, these methods are accompanied by time-consuming sample preparation, the use of expensive and hazardous solvents, and the need for skilled personnel to execute the intricate procedures, emphasizing the importance of exploring the development of more accessible, swift, and cost-effective techniques for detecting HA in body fluids.[26]

Application of colorimetric-based analytical methods has emerged as an low-cost and effective technology to address previously challenges about sensing of HA. The colorimetric detection of markers utilizing nanoparticles, particularly AgNPs, has gained popularity owing to their heightened sensitivity.[27] These nanoparticles possess distinct optical characteristics determined by their dimensions, configuration, and arrangement, rendering them well-suited for detecting a wide range of target molecules such as DNA, microRNA, proteins, and more.[28]

Using commercially available plates or boxes in a plate reader for colorimetric analysis with nanoparticles may incur high costs, limit portability, and depend on sample volume. Consequently, there is a requirement for an affordable substrate for marker colorimetric analysis. This has prompted the investigation of incorporating nanoparticle-based sensors into paper-based micro-pads to address these issues, as they present cost-effective, swiftly producible, with low sample volume requirements, and portable solutions.[29]

Recently, there has been a rising inclination towards the utilization of digital technology for analysis.[20] This includes obtaining and digital images to speed up the analysis and eliminate the requirement for expensive equipment on the semi-analytical studies. The digital images are obtained through the interaction of radiation with the sample, resulting in absorption and reflection of the radiation. The utilization of colorimetric reactions is especially captivating for digital image-based methods, as when a colored reaction product is exposed to visible light, it reflects radiation. Smartphones can take pictures that can be transformed into color patterns using the red (R), green (G), and blue (B) models, defined by the International Color Consortium (ICC).[30] Therefore, any changes in color is characterized on a scale ranging from 0 to 255 (8-bit format) or 0–1 (fractional format). Image processing software, such as Photo Metrix apps, is employed to ascertain the intensity of the measured R, G, and B channels in the captured digital image.[31] Consequently, the intensity of color obtained from the pictures corresponds to the level of concentration of the resultant-colored substance formed from the interaction of the analyte and the reagent. Utilizing digital images allows for the
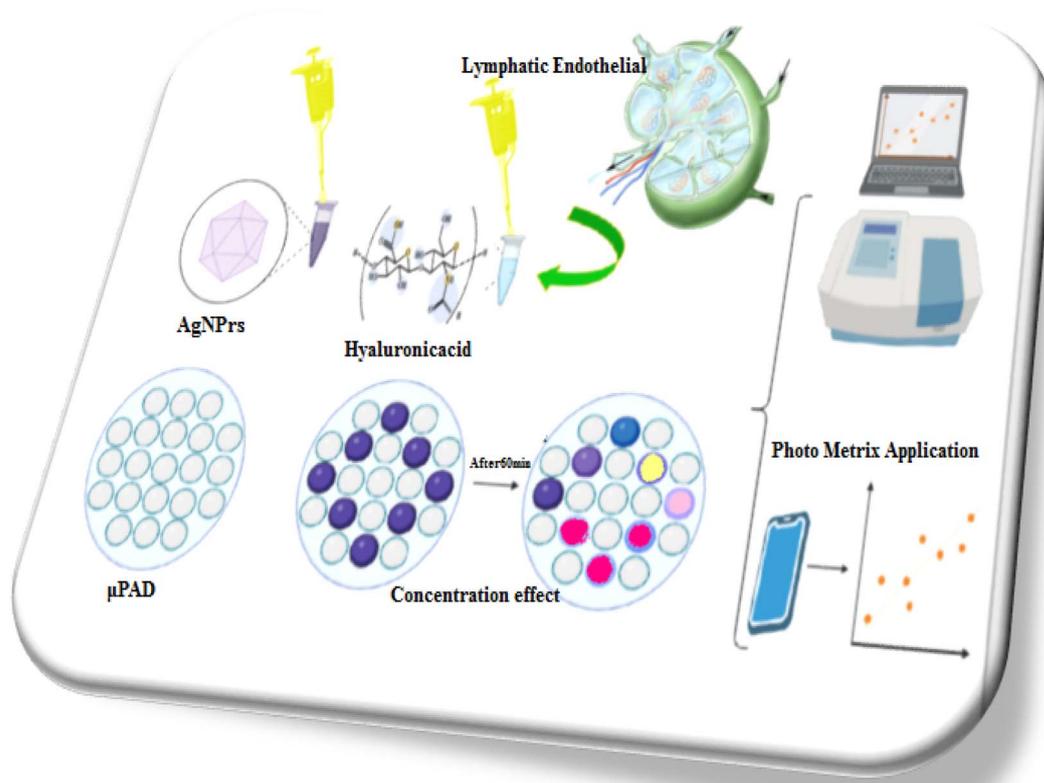
Scheme 1 Illustration of the fabrication and detection process of HA using triangular TA-AgNPrs with RGB analyze and μPAD.

substitution of costly analytical methods. Furthermore, digital image-based approaches facilitate decreased utilization of reagents and samples, swift analysis, automation, and portability.[32]

This study presented a novel and cost-effective colorimetric detection method to monitor HA in real human samples using TA-AgNPrs as an optical probe. The results were evaluated using UV-Vis spectroscopy and a colorimetric approach, incorporating micro-pads to detect low levels of HA in real samples. Furthermore, the research explored HA detection in human real samples using the RGB method (digital images analysis) taken with smartphones. The findings were assessed using colorimetric techniques, employing μPAD for optical monitoring of HA in human biofluids. Scheme 1 illustrates the optical and photochemical detection of HA in real samples.

2. Experimental details

2.1. Reagents and materials

Cysteine (Cys), ascorbic acid (AA), uric acid (UA), proline (Pro), aspartic acid (As), methionine (Met), histidine (His), glycine (Gly), and alanine (Ala) were obtained from Merck, Germany. In addition, Acetonitrile was also purchased from the same vendor. Silver chloride (AgCl), silver nitrate (AgNO$_3$), sodium borohydride (NaBH$_4$), trisodium citrate (Na$_3$C$_6$H$_5$O$_7$), hydrogen peroxide (H$_2$O$_2$), and polyvinyl pyrrolidone (PVP) K-30 were acquired from Sigma Aldrich, Canada. The deionized water used in the experiments was provided by Ghazi Pharmaceutical Company in Tabriz, Iran. Lastly, glass fiber sheets were procured from Whatman Co, Germany.

2.2. Instrumentation

To analyze the size and the zeta potential, Zetasizer Ver (Malvern Instruments Ltd.) (UK), MAL1032660 was utilized. To control the brightness and avoid being affected by external radiation, a box with a diameter of 8.0 cm and a height of 10 cm was made of black PLA, and the pictures were captured with autofocus and the free Photo Metrix app.

2.3. Synthesis of silver nanoprisms

The AgNPrs were synthesized as previously described.[33]

2.4. Real sample preparation

Samples of human blood serum were generously provided by the Iranian Blood Transfusion Research Centre in Tabriz, Iran. Additionally, human urine samples were collected from healthy, drug-free volunteers. The blood serum samples underwent centrifugation with acetonitrile at a speed of 8000 rpm for 10 min to obtain the supernatant, which was then stored in a 2 ml vial for colorimetric and spectrophotometric analysis. Conversely, the urine samples were left untreated and only diluted with distilled water in a 1 : 1 ratio. Moreover, this study received technical support from the Pharmaceutical Analysis Research Centre at Tabriz University of Medical Science.

2.5. Construction of micro-PAD (μPAD)

The microfluidic sample in this study was prepared by transferring it from a paraffin-coated fiberglass sheet to a clean fiberglass sheet using a hot iron mold to create the μPAD. Subsequently, this device was employed to quickly and conveniently detect HA in blood plasma and urine samples through the use of silver nanoprisms for colorimetric analysis. There are different approaches to fabricating paper sensors, and one of them involves utilizing wax transfer for colorimetric analysis.[34] The rationale for utilizing wax lies in its affordability, wide availability, and environmental friendliness. This technique necessitates a wax printer and low-cost printing plates. It is worth noting that wax screen printing presents a straightforward and cost-effective way of creating μPAD. In this uncomplicated method, wax patterns are printed onto the paper surface through a simple screen-printing process. Importantly, the wax printing process does not require a sterile room, a UV lamp, organic solvents, or sophisticated equipment. Another significant advantage of this approach over preceding methods is its ability to be executed anywhere globally on a typical hot plate, making it a novel method for producing μPADs.[35] So, engineered platform can be utilized for colorimetric-based analytical studies. Paper microfluidics, or lab on paper, is a burgeoning field of study that commenced in 2007 and continues to expand. Paper microfluidics represents a fresh system for fluid transport and analysis catering to numerous applications.[36]

The movement of wax into paper occurs due to capillary forces without the need for external forces or pumps. Presently, the paper-based microfluidic system is gaining attention as an affordable, user-friendly, disposable, and equipment-free technology, with potential to enhance healthcare, disease treatment, and screening particularly in underserved regions. It is recognized that there are disparities in access to medical and health education globally. The sensitivity and selectivity of this method have been confirmed through the testing of HA in the presence of potential interferences. Furthermore, a novel, portable, and cost-effective substrate-based technique has been suggested for analyzing HA in human fluids. To the best of our knowledge, there is no reported uses of TA-AgNPrs-decorated μPADs for HA detection, making it a comparison worth considering.[37]

The efficiency of papers was assessed using TLC paper, and the findings indicated that glass fiber paper experiences less abrasion due to its superior flow behavior. Paraffin, through its interaction with a chromogen in the detection zone, can be utilized to identify the target, driven by the color produced by the excited product. This approach offers various advantages, including a low melting point, cost-effectiveness, and thermoplasticity. Moreover, paraffin wax, a primary waste product in wax printing, is commonly employed to produce μPAD and demonstrates resistance to most materials utilized in the study.[38] Standard μPADs are created through wax printing techniques, resulting in the formation of a micro-zone within the paper model. The advancement of μPAD technology enables the simultaneous analysis of multiple samples,

simultaneously.[39] The mold is heated to a temperature of 90 °C, and the corresponding piece of paper is placed into it for a duration of 30 seconds. After drying, the iron sample is then heated for two minutes at a temperature of 150 °C. The paper is placed between the magnet and iron mold. Consequently, the paraffin diffused into the paper's composition which led to providing of hydrophilic channels on the surface of paper.

Additionally, in conjunction with the µPAD, parafilm was employed for applying droplets. After being melted at 90 °C, the paper in question was submerged in the substance for 30 seconds, and then heated at 85 °C for 10 seconds after drying. By placing a parafilm sheet between the iron pattern and the magnet, paraffin can permeate the parafilm structure, resulting in the creation of hydrophilic channels on the surface. Once prepared and dried, the µPADs were ready for colorimetric analyses. Parafilm, a thin, semi-transparent sheet, is highly pliable and classified as a thermoplastic polymer. Thermoplastics, essentially, maintain their chemical composition even after they have been melted and cooled, displaying no alteration in their material characteristics. Parafilm is flexible, thermoplastic, and chemically conductive.

The detection of HA was accomplished using a µPAD modified with optical nanoprobes TA-AgNPrs. Therefore, the proposed technique signifies the first stage in the development of HA diagnostic kits that deliver superior qualitative outcomes and undergo rapid, cost-effective color alterations. Paraffin's infiltration into the paper's structure yields a hydrophilic layer on its surface (Scheme S1 and Video – see ESI†).

3. Results and discussion

3.1. Confirmation of HA reaction with TA-AgNPrs using color change, UV-Vis method

TA-AgNPrs display a high level of anisotropy and demonstrate distinctive UV-Vis wavelengths. The UV-Vis spectra of AgNPrs, with 0.02 M of HA, and AgNPrs following the introduction of HA at varying incubation periods were tested (Fig. 1). It is evident that the LSPR peaks for AgNPrs were observed at 646 nm and 585 nm immediately and after 60 min, respectively. Combining the TA-AgNPrs solution with HA (0.02 M) resulted in

a significant decrease in the intensity of the UV/Vis peaks. The most notable shift in wavelength occurred at 592 nm after a 60 minute incubation period. Triangular AgNPrs exhibit exceptional anisotropy and display distinctive LSPR features with a high extinction coefficient. The alteration in the morphology of TA-AgNPrs is the primary cause of the blue shift and color change of the opto-probe. Upon the introduction of HA, the triangular AgNPrs transformed into circular nanodisks, causing the color to transition from blue to yellow, reflecting the sensitivity of the HA interaction with these triangular AgNPrs. Based on colorimetric and spectrophotometric analyses, it is evident that HA coordinated with TA-AgNPrs, consequently leading to the recognition of HA's influence.

For further investigation, the zeta potential (Z_p) of the optical probe was measured under various conditions, both in the absence and presence of the analyte. Initially, the Z_p of TA-AgNPrs (the optical probe) was determined to be −14.6 mV with a conductivity of 13.8 mS cm^{-1}. Upon interaction with HA, the Z_p remarkably increased to −0.749 mV, while the conductivity decreased to 1.21 mS cm^{-1}. After a 5 minute incubation period, the Z_p further increased to 7.88 mV, and the conductivity reached 0.977 mS cm^{-1}. These results confirm the successful interaction between HA and the optical probe, demonstrating the effectiveness of the proposed method for identifying the target analyte. Notably, the reaction kinetics of HA with TA-AgNPrs are rapid, with the reaction completing within the first minute of mixing the probe with the target molecule. Furthermore, DLS results indicated an average particle size of 68.80 nm for TA-AgNPrs (Fig. S1, ESI†). The prepared TA-AgNPrs solution displayed a brilliant sea blue color with a spectrophotometry absorption peak at 526 nm. Additionally, TA-AgNPrs exhibited UV/vis emission within the 400 to 600 nm range. UV-Vis spectra revealed a maximum absorption for TA-AgNPrs at approximately 526 nm. Upon interaction with HA, the solution's color promptly changed to yellow. As a result, an increase in the concentration of HA triggers the aggregation of numerous TA-AgNPrs particles, leading to a noticeable color change.

Following the initial assessment of the engineered system for HA detection in the solution, µPADs were employed for the
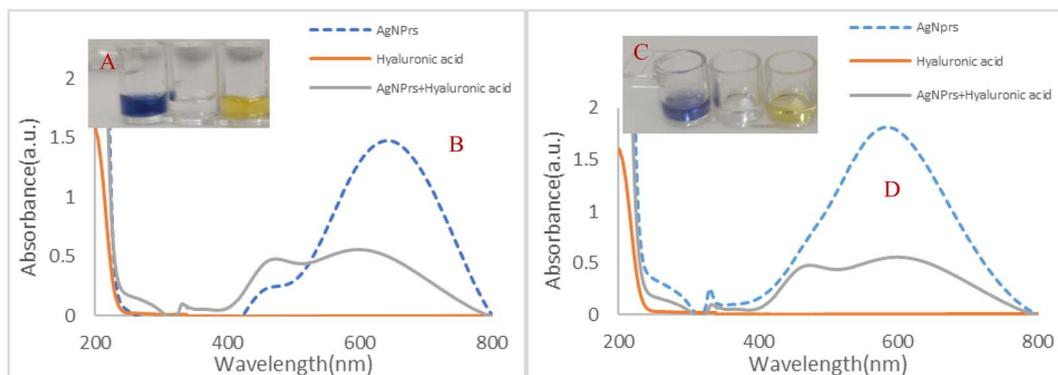

Fig. 1 (A and C) Photographic images and (B and D) UV-Vis spectrum of (1) AgNPrs, (2) HA 0.02 M and (3) TA-AgNPrs/HA 0.02 M (1 : 1 v/v) in reaction times of 0 and 60 min, respectively. Solvent; deionized water.

portable monitoring of HA on the μ-zone of the substrate. To conduct the colorimetric assay of HA with the μPAD paper, the μ-zone underwent preparation and examination. In the first trial, the μ-zone network was created with 30 seconds of heat and pressure on the fiberglass paper. Subsequently, it took nearly 60 minutes for a drop of TA-AgNPrs and HA to react until they were either absorbed into the paper or dried. Upon injecting AgNPrs and HA, a noticeable color change occurred in the detection zone of the injected areas (Fig. 2A–C). This modification in the preparation of the μPADs rendered it suitable for AgNPrs-based colorimetric systems employing a time/color shift system (Video, ESI†).

Based on the results obtained, the established approach successfully detects HA. Therefore, we devised this colorimetric/spectrophotometric sensor method to quantify HA in standard solutions and human biofluids.

3.2. Analytical study

To quantify the concentration of HA, colorimetric and UV/vis methods were employed. Various analyte concentrations ranging from 0.5 μM to 30 mM were prepared in deionized water, followed by the addition of TA-AgNPrs at a 1 : 1 v/v ratio. The resulting mixtures were promptly photographed at 0 minutes and then again after 60 minutes once the reaction had reached completion. At the start of the analysis (0 min), HA concentrations of 30, 20, 10, and 5 mM induced an observable change in the blue color of the TA-AgNPrs, indicating the initiation of interaction with the target molecule. After 60 minutes, the color of the HA changed to a pale yellow, confirming complete reaction of the optical probe with the analyte. These results underscore the method's ability to detect HA at varying concentrations, validating the time-dependent interaction of HA with TA-AgNPrs. Subsequently, the kinetics of this reaction become notably crucial. As per these findings, the naked-eye would be capable of discerning the presence of HA at concentrations as low as 0.03, 0.02, 0.01, 0.005, and 0.002 M in a standard solution (Fig. 3). The latter part of the investigation focused on scrutinizing the UV-Vis spectra of standard samples following a 60 minute incubation with TA-AgNPrs, considering the relatively stable color at that point. To determine the range of the analyte's determination using the proposed chemo-sensing technique, we plotted histograms of absorbance *versus* HA concentration at different incubation times (0 and 60 minutes) and a histogram of the peak position (wavelength). The results showed that HA with concentrations of 0.03, 0.02, 0.01, 0.005, and 2 mM can induce a shift in the absorption band spectrum. The calibration curves (Fig. 3(E) and (F)) yielded regression equations of Abs (a.u) $= -15.065(C_{HA}) + 0.9139$, $R^2 =$
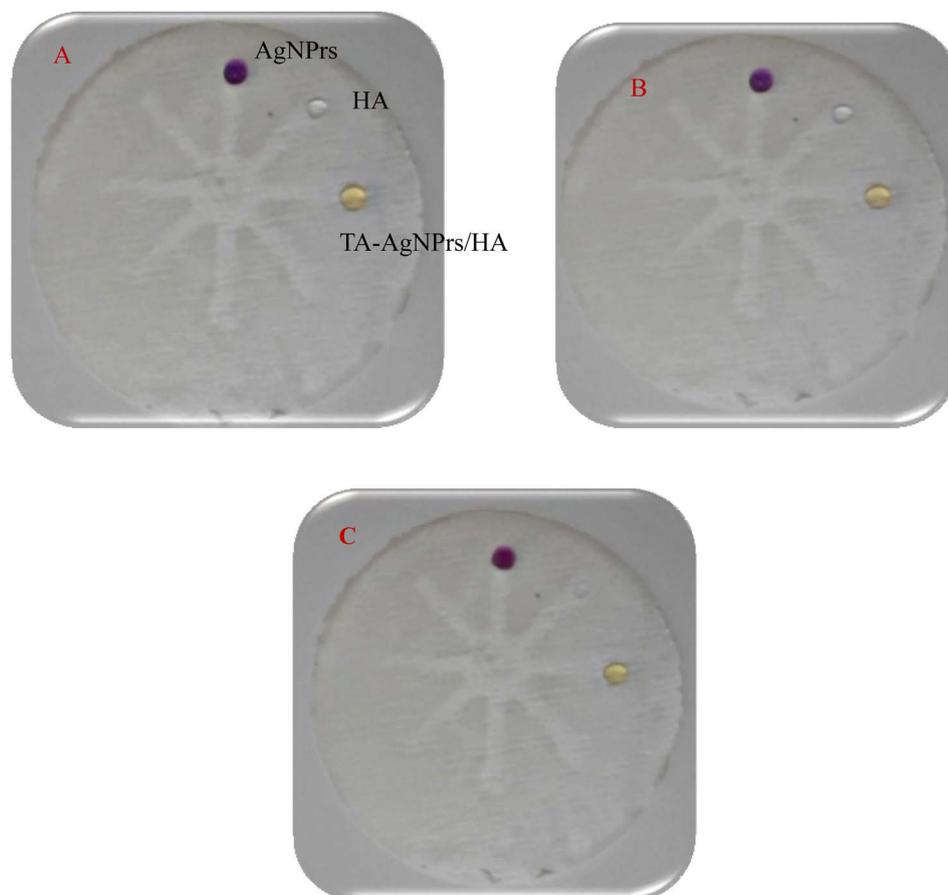

Fig. 2 Photographic images of μPAD for TA-AgNPrs, HA, and TA-AgNPrs/HA (1 : 1 v/v) in the incubation time of 0 min (A), 30 min (B), and 60 min (C).
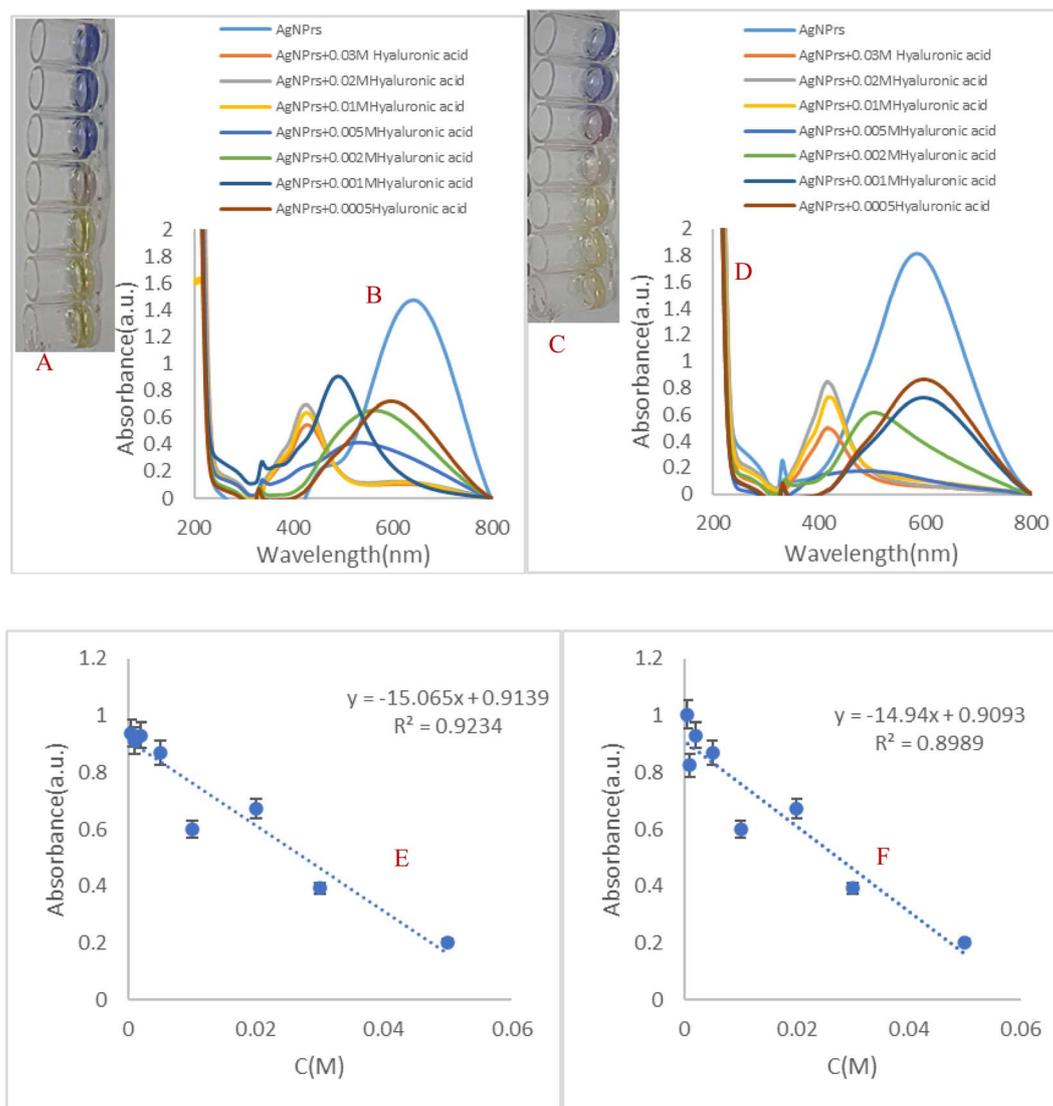
Fig. 3   (A and C) Colorimetric response of TA-AgNPrs to HA in different concentrations and various incubation times 0 and 60 min, respectively. (B and D) UV-Vis spectra of opto-sensor for different concentrations of HA in different incubation times of 0 and 60 min, respectively. (E and F) Calibration curves in different incubation times of 0 and 60 min, respectively.

0.9234 for 0 minutes and Abs (a.u) $= -14.94(C_{HA}) + 0.9093$, $R^2 = 0.8989$ for 60 minutes, demonstrating a linear relationship between absorbance and wavelength with HA concentrations in the range of 5 to 30 mM. Based on the data, the proposed colorimetric strategy utilizing TA-AgNPrs exhibits a significant response for the determination of HA, with a low limit of quantification (LLOQ) of 5 mM. Based on the results, the suggested optical sensing approach can accurately detect HA with sensitivities of 15.065 and 14.94 (a.u M^{-1}) at different reaction times of 0 and 60 minutes, respectively.

3.3.   Analytical approach

To enable the convenient and on-site analysis of HAs using paper-based colorimetric and digital image analysis, we proposed and assessed the µPADs. Our device is constructed using a straightforward, cost-effective, and adaptable wax molding machine. We conducted experiments on both paper and parafilm substrates. Parafilm consists of thin, translucent sheets categorized as flexible and thermoplastic polymers. Thermoplastics are defined as polymers that withstand hot and cold conditions, melt while maintaining the same chemical composition, and return to their original state after cooling; they do not decompose at high temperatures but only change their shape, structure, and composition. The substrate contains 37 square zones for the analysis of 37 samples. On the next step, 5 µL of TA-AgNPrs were applied to each area, followed by the addition of 5 µL of the analyte. Zone 1 was dedicated to TA-AgNPrs, while zones 2 and onwards were exposed to HAs with concentrations varying from 0.5 µM to 30 mM (refer to Fig. S2 and Video, see ESI†).

Initially, it was observed that the sensing zone experiencing high concentrations of HA (0.03, 0.02, 0.01, and 5 mM) underwent a more rapid color change compared to the other sensing zones (Fig. S2, ESI†). Hence, for the semi-quantitative analysis

of HA, the color change over time can serve as an indicator of the analyte. It is worth noting that remarkable results were obtained on paper substrates, while paraffin substrates displayed similar colors to those of paper substrates. The calibration curves of the optical chemosensor were depicted in Fig. S2 and the Video (ESI†), using RGB analysis, with a volume ratio of 1 : 1. Linear regression analysis of the collected data resulted in R^2 values of 0.8675. As per Lambert's law, the amount of light absorbed by different solution layers remains constant and does not depend on the intensity of the emitted light.

Based on the laws of Beer and Lambert, the relationship between a solution's concentration and the absorption of light is usually linear. Typically, substance concentrations are determined in the range where absorption shows a linear relationship with concentration.[38] The experiment provided details the process of carrying out absorbance measurements and analyzing Beer's law using a simple protocol. In this case, a cell phone application called the Photo Metrix analyzer is used as a light detector, capable of determining the average RGB value of images in real time. The light source utilized can be either light reflected from colored construction paper or light from a computer screen. In summary, a chemical analysis of HA is executed with an OD strategy to minimize reagent consumption, specifically of analyte and solvent, in monitoring HA. As a result, a small and portable kit was created for the recognition of specific HA.

3.4. Real sample analysis

To evaluate the effectiveness of the developed method for HA monitoring in real samples, we utilized the engineered system to detect the analyte in human serum and urine samples. To assess the method's appropriateness for human samples, serum samples were treated with a 1 : 1 v/v mixture of acetonitrile, then centrifuged for 10 minutes. The resulting supernatant was combined with HA and the optical probe at a volume
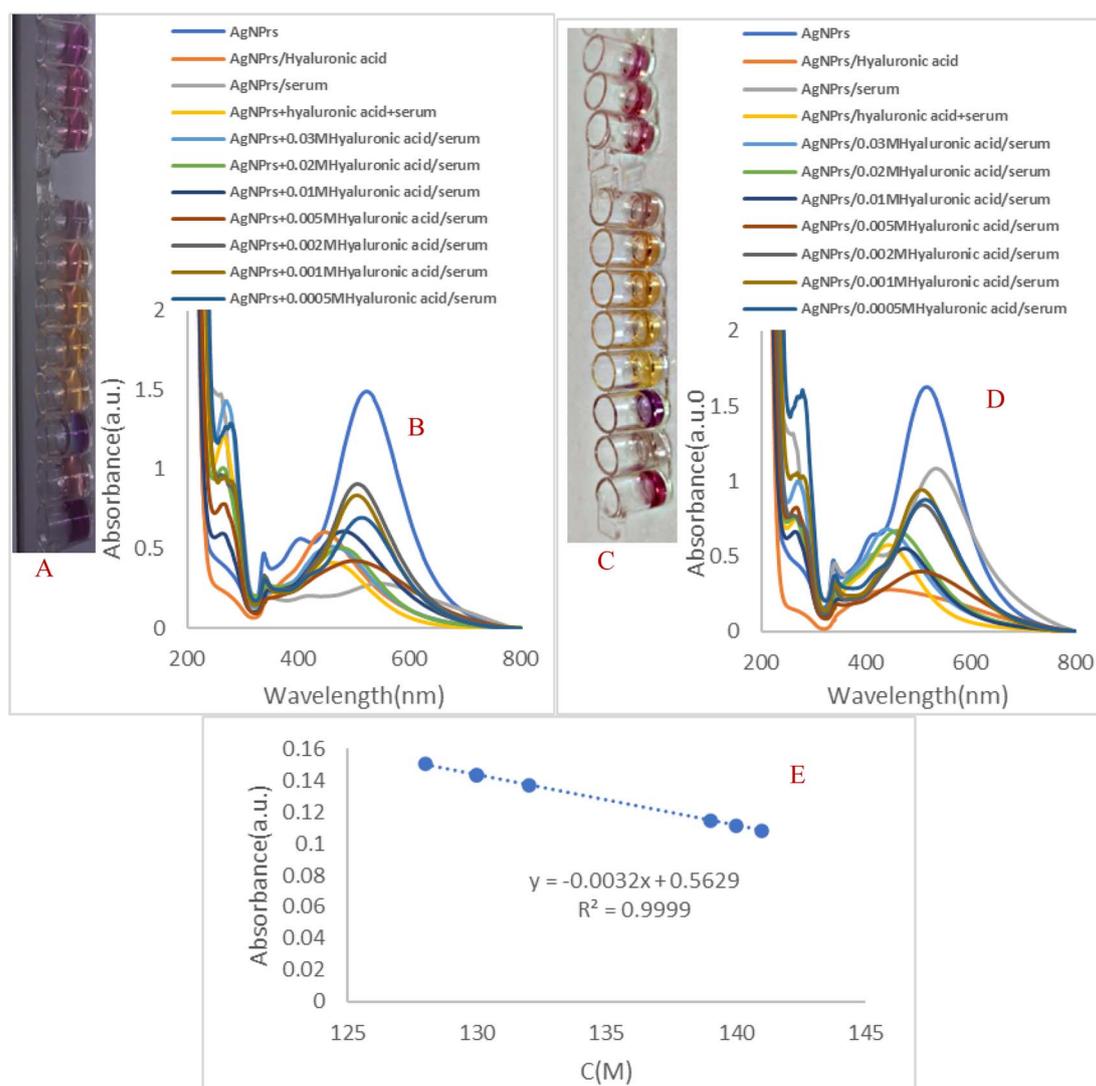

Fig. 4 (A and C) Photographic images for colorimetric determination of HA (0.03, 0.02, 0.01, 0.005, 0.002, 0.001, 0.0005 M spiked in human serum sample). (B and D) UV-Vis spectrum of TA-AgNPrs after interaction with different concentrations of HA (0.03, 0.02, 0.01, 0.005, 0.002, 0.001, 0.0005 M). (E) Calibration curve.

ratio of 1 : 0.5 : 0.5 v/v/v, as depicted in Fig. 4. A visual inspection revealed a reduction in the color intensity of TA-AgNPrs after adding HA to the serum, despite the presence of HA. UV-vis spectroscopy analysis further verified these observations, displaying minimal shift in the peak area and absorption of TA-AgNPrs/treated human serum in the existence of HA (Fig. 4). The findings were in alignment with the UV-visible spectrum, further validating the colorimetric results. The histogram shows absorbance from the opto-sensor against HA/TA-AgNPs, TA-AgNPs/serum, HA/TA-AgNPs/serum at two different incubation times (0 and 60 min), as well as the calibration curves of the opto-sensor in human serum sample, as depicted in Fig. 4. Importantly, the regression equation Abs (a.u) = $-0.0032C_{HA}$ + 0.5629 (R^2 = 0.9999) was established for HA within the concentration range of 5 to 30 mM, confirming the relationship between wavelength and analyte concentration.

The study also examined the presence of hyaluronic acid (HA) in human urine samples using a specially designed optical chemosensor. The urine sample was purposely enriched with varying concentrations of HA (ranging from 5 to 30 mM) in combination with TA-AgNPrs as the optical sensing probe, with a volume ratio of 1 : 0.5 : 0.5 v/v/v. Subsequent colorimetric and UV/Vis data were captured and analyzed (Fig. S3, ESI†). Upon visual inspection, it was observed that the color intensity of AgNPrs dissipated following the addition of urine, regardless of the presence of HA. Importantly, UV-Vis assisted opto-analysis also confirmed these findings and indicated minimal shift in the area intensity of absorption peak of TA-AgNPrs/urine in the existence of HA (Fig. S3, ESI†). These outcomes aligned with the UV-visible spectrum observations, reaffirming the results obtained via colorimetric analysis. The absorbance histogram of the opto-sensor in relation to HA/TA-AgNPs, TA-AgNPs/urine, and HA/TA-AgNPs/urine at two different incubation durations (0 and 60 minutes) and the calibration curves are depicted in Fig. S3 (ESI†). Notably, the equation Abs (a.u) = $-1.7236C_{HA}$ + 0.1387 (R^2 = 0.8973) was derived within the HA concentration range of 2 to 20 mM, confirming the correlation between wavelength and concentration.

Based on the results obtained, the suggested method has demonstrated the ability to alter HA in human biofluids. Consequently, HA was introduced into human urine and subjected to µPCD analysis. In this regard, various concentrations of HA at a v/v ratio of 1 : 1 (5 mM to 20 mM) were employed, and colorimetric analysis was conducted. The RGB analysis indicated an interaction between the urine-HA mixture and TA-AgNPs. However, the absorbance of the opto-sensor did not align with the HA concentration (Fig. S4 and S5, ESI†). As illustrated in Fig. S4,† a linear correlation was observed in the calibration curve of peak versus HA concentration in the human urine sample within the range of 5 to 20 mM and an incubation time of 60 min, yielding an R^2 value of the regression equation as 0.9631 (further details available in the ESI Video†). Subsequently, the engineered chemosensor was utilized to detect HA in human serum samples using µPCD. The serum samples were mixed with acetonitrile at a 1 : 1 v/v ratio, subjected to centrifugation for 10 minutes, and then the supernatant was collected and analyzed after the addition of TA-AgNPrs as an optical

sensing probe and various concentrations of HA (5 to 100 mM) at a v/v ratio of 1 : 1 (Fig. S4, ESI†). Notably, RGB analysis detected an interaction between diverse concentrations of HA and TA-AgNPrs in the human urine sample. Fig. S5 (ESI†) illustrates the histogram and calibration curve of peak versus HA concentration in the serum sample, covering the range from 5 to 100 mM, recorded over an incubation period of 60 minutes. The calibration curve yielded a regression of Abs (a.u) = -8.066 + 0.133 (R^2 = 0.937) (details available in the ESI Video†).

3.5. Repeatability and reproducibility

To assess the optical method for quantifying hyaluronic acid (HA), the consistency was studied over a 60 min interval using three different HA concentrations (high, medium, low) measured at different incubation times (20, 40, and 60 min), and the outcomes were depicted in Standard Deviation (SD). As illustrated in Fig. 5, the UV-Vis spectrum findings reveal minimal variations in the three absorption bands. Despite a gradual decrease in band intensities, the reduction ratios were consistent across all, without impacting their wavelength positions. These findings verify the robustness of the tests.

The above information reveals that UV-Vis spectra measurements were conducted for a substance at various concentrations over a 1 hour timeframe, involving high, medium, and low concentrations. Following the initial measurement, the data analysis focused on assessing the standard deviation (SD) values associated with each concentration level and time point. Here's how to interpret the results:

SD for 0.02 M:

● The SD is around 0.034359, indicating moderate variation around the mean wavelength of 447 nm for this concentration.

● 0.002 M: the SD is approximately 0.010275, suggesting low variation around the mean wavelength of 498 nm.

● 0.0005 M: the SD is roughly 0.016307, similar to the 0.002 M concentration, implying low variation around the mean wavelength of 489 nm.

In summary, the SD values offer insights into the consistency and variability of the measurements. Lower SD values signify closely clustered measurements around the mean, reflecting higher precision and reliability. Conversely, higher SD values signal more scattered measurements, indicating greater variability in the data.

3.6. Selectivity analysis of HA using µPCDs decorated by TA-AgNPrs

To done the selectivity of the developed technique for recognition of HA, a combination of AgNPrs/HA and interfering agents (in a 1 : 0.5 : 0.5 v/v/v ratio) was introduced to each detection zone from 1 to 10 (Fig. S6 and Video, see ESI†). Initially, the sensing zones of µPCDs were treated with AgNPrs and then with various combinations of AgNPrs/HA/Gly, AgNPrs/HA/Cys, AgNPrs/HA/Met, AgNPrs/HA/Pro, AgNPrs/HA/Phenyl, AgNPrs/HA/Aspartic acid, AgNPrs/HA/Ascorbic acid, AgNPrs/HA/Dopamine, and AgNPrs/HA/Urea. After 60 minutes, the results were examined. As depicted in Fig. S7 and the accompanying Video in the ESI,† the established method demonstrates
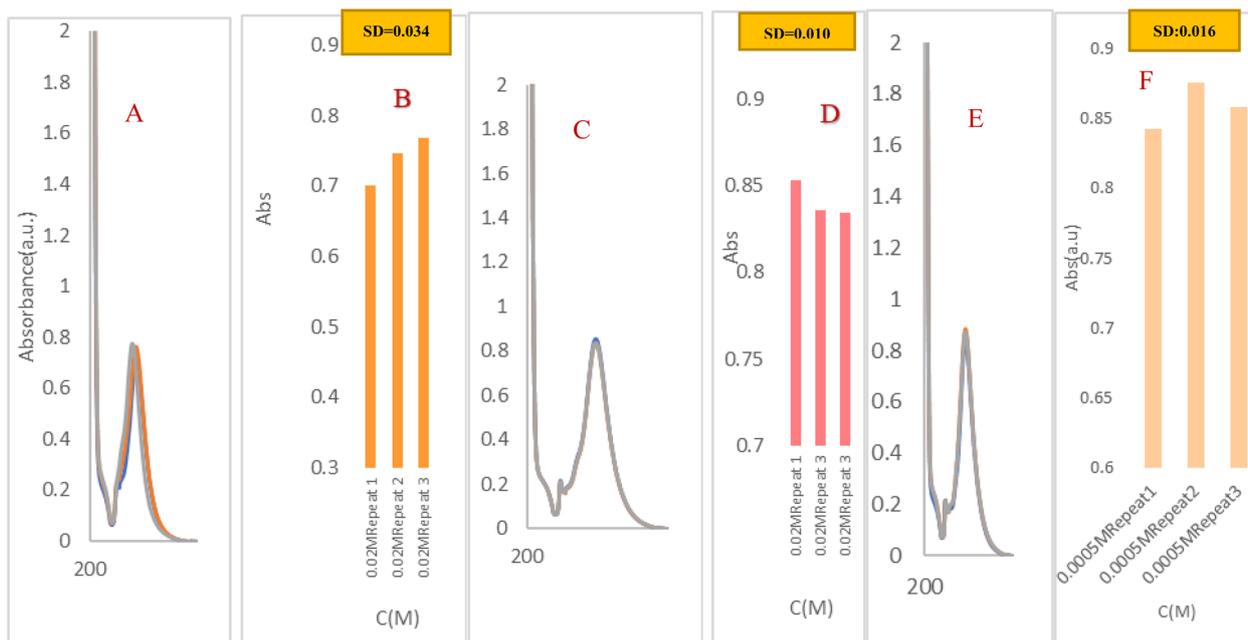
Fig. 5 (A, C and E) UV-Vis spectral of opto-sensor for HA recognition in different interaction time of 0 to 60 min in different repetition time (20, 30, and 40 min). (B, D and F) Histogram of absorption intensity *versus* both incubation time/number of repeat.

Table 1 Material/analytical comparison of previously opto-sensing-methods for the monitoring of HA

Method	Nano probe, nano-polymer, biomarker	LOD/LOQ	Linear range	Ref.
Fluorescence spectroscopy	HAPPF@FeSe$_2$ NPs	1.50 (f)	1.5–5.2 ppm	40
Fluorescence spectroscopy (FRET)	CSTPP/HA-R nano gels	1.2 ppm	2.40×10^{-10} m^2 s^{-1}, 1.8×10^{-11} m^2 s^{-1}	41
Surface-enhanced Raman spectroscopy (SERS)	HA-AuNPs	0.4 mU mL^{-1}	10^{-3} to 10^{-2} U mL^{-1}	42
HA-AuNP@SiNP-based fluorometry	HA-AuNPs@SiNPs nano probe	0.004 U mL^{-1}	0.01 to 10 U mL^{-1}	43
Enzyme-linked immunosorbent assay	PCA3, HAase and HA	24 000 U mL^{-1}	0–240 000 U mL^{-1}	44
NR, cationic CD-based fluorometry	C-CDs	50 U mL^{-1}	100–80 000 U mL^{-1}	45
µPAD integrated spectrophotometry	AgNPrs	0.0005 M	0.03–0.0005 M	This work

selectivity for HA detection even in the presence of active components. Further analysis of Fig. S6 and S7† indicates that there is no reaction between the interfering species and the optical probe in the absence of HA, resulting in their inactivity in the engineered sensing strategy for HA detection.

Table 1 presents a comparison of the analytical performances of different methods for detecting HA, such as Fluorescence spectroscopy, FRET, surface-enhanced Raman spectroscopy (SERS), ELIZA, and NR, with the recommended approach in this report, which is based on cationic CD.[40–45]

According to the data from previous reports (Table 1), most commonly described techniques have several limitations, such as low sensitivity, complex mobile phases, and time-consuming extraction procedures with limited adaptability. A comparison of the findings from this study with previously documented methods indicates that the developed approach offers several advantages, including the stability of the optical probe, an appropriate surface area, and practical biological activity. The majority of techniques for identifying HA rely on fluorimetry,

with spectrophotometry being infrequently utilized. The unique and innovative aspect of the present study lies in its cost-effectiveness, quick implementation, practicality, and sensitivity. Obtained results are confident that the developed approach can serve as a reliable assay for quantitatively determining HA in real samples. Our study's strength lies in using the colorimetric µPAD for real-time, on-site HA determination in real samples, which is also cost-effective, quick to operate, portable, and provides rapid results.

4. Conclusions

In summary, the use of TA-AgNPrs for optically detecting HA was assessed. The analytical findings for the proposed TA-AgNPrs based colorimetric chemosensor are consistent with previously reported results, showing a wide linearity range of 0.0005–0.03 M and a suitable LLOQ of 0.5 mM. Notably, TA-AgNPrs demonstrated successful detection of HA in real human samples, with improved specificity in the presence of

various interfering agents. Leveraging these advantages in data processing, this research presents innovative potential for the development of straightforward and efficient semi-quantitative analytical devices. Implementation of real-time on-site HA detection in a portable device is poised to revolutionize research in this field. Additionally, the integration of microfluidic paper-based colorimetric devices (μPAD) with smart devices, such as smartphones, opens up possibilities for personalized medicine. These findings highlight the significant potential of TA-AgNPrs as a stable and cost-effective sensing substrate for highly sensitive HA detection. It is hoped that the experimental process can lead to modifications in μPAD preparation, specifically focusing on liquid HA in the human body. The chemosensor developed in this study will show ongoing improvement in performance. The innovative design of the sensor, utilizing original bio functionalized surface immunity, will result in a highly resilient biosensor with exceptional sensitivity and specificity, capable of rapid detection of HA in complex samples. These biosensors will have widespread applications in environmental monitoring, clinical drug discovery, diagnostics, and food quality control.

Data availability

Access to the data used in this study is available upon request and may be subject to approval by the data provider. Restrictions may apply to the availability of these data, which were used under license for this study. Interested parties are encouraged to contact the corresponding author for further information on accessing the data. All relevant data supporting the findings of this study are available within the article and its ESI,† or from the corresponding author upon reasonable request. Access to some data may be restricted due to privacy or ethical restrictions. Any restrictions to data availability will be disclosed at the time of data request.

Conflicts of interest

There are no conflicts to declare.

Acknowledgements

References

1 S. Saha, F. Fan, L. Alderfer, F. Graham, E. Hall and D. Hanjaya-Putra, *Biomater. Sci.*, 2023, **11**, 7346–7357.

2 W. Lawrance, S. Banerji, A. J. Day, S. Bhattacharjee and D. G. Jackson, *J. Biol. Chem.*, 2016, **291**, 8014–8030.

3 K. Solakyildirim, *Advanced Analytical Techniques in Glycosaminoglycan Analysis*, Rensselaer Polytechnic Institute, 2012.

4 G. Kogan, L. Soltes, R. Stern and R. Mendichi, *Handbook of Polymer Research: Monomers, Oligomers, Polymers and Composites*, ed. R. A. Pethrich, B. Antonio and G. E. Zaikov, 2007, pp. 393–439.

5 S. K. Hahn, J. K. Park, T. Tomimatsu and T. Shimoboji, *Int. J. Biol. Macromol.*, 2007, **40**, 374–380.

6 A. Panagopoulou, J. V. Molina, A. Kyritsis, M. M. Pradas, A. V. Lluch, G. G. Ferrer and P. Pissis, *Food Biophys.*, 2013, **8**, 192–202.

7 N. M. Salwowska, K. A. Bebenek, D. A. Żądło and D. L. Wcisło-Dziadecka, *J. Cosmet. Dermatol.*, 2016, **15**, 520–526.

8 K. Vorvolakos, J. C. Coburn and D. M. Saylor, *Soft Matter*, 2014, **10**, 2304–2312.

9 Z. Zhang and G. F. Christopher, *Soft Matter*, 2015, **11**, 2596–2603.

10 Y. Kobayashi, A. Okamoto and K. Nishinari, *Biorheology*, 1994, **31**, 235–244.

11 S. Fusco, A. Borzacchiello, L. Miccio, G. Pesce, G. Rusciano, A. Sasso and P. A. Netti, *Biorheology*, 2007, **44**, 403–418.

12 M. I. Tammi, A. J. Day and E. A. Turley, *J. Biol. Chem.*, 2002, **277**, 4581–4584.

13 A. Mráček, J. Varhaníková, M. Lehocký, L. Gřundělová, A. Pokopcová and V. Velebný, *Molecules*, 2008, **13**, 1025–1034.

14 C. Spagnoli, A. Korniakov, A. Ulman, E. A. Balazs, Y. L. Lyubchenko and M. K. Cowman, *Carbohydr. Res.*, 2005, **340**, 929–941.

15 M. F. Graça, S. P. Miguel, C. S. Cabral and I. J. Correia, *Carbohydr. Polym.*, 2020, **241**, 116364.

16 H. P. Schneider and A. Landsman, *Wounds*, 2019, **31**, 41–48.

17 M. G. Neuman, R. M. Nanau, L. Oruña-Sanchez and G. Coto, *J. Pharm. Pharm. Sci.*, 2015, **18**, 53–60.

18 M. N. Collins and C. Birkinshaw, *Carbohydr. Polym.*, 2013, **92**, 1262–1279.

19 M. Litwiniuk, A. Krejner, M. S. Speyrer, A. R. Gauto and T. Grzela, *Wounds*, 2016, **28**, 78–88.

20 E. Ahmadian, S. M. Dizaj, A. Eftekhari, E. Dalir, P. Vahedi, A. Hasanzadeh and M. Samiei, *Drug Res.*, 2020, **70**, 6–11.

21 C. A. Cooper, K. K. Brown, C. D. Meletis and N. Zabriskie, *Alternative Compl. Ther.*, 2008, **14**, 78–84.

22 M. Šimek, K. Lemr, M. Hermannová and V. Havlíček, *Carbohydr. Polym.*, 2020, **250**, 117014.

23 J. Sun, G. Wang, H. Cheng, Y. Han, Q. Li and C. Jiang, *Bioelectrochemistry*, 2022, **145**, 108073.

24 M. Ge, J. Sun, M. Chen, J. Tian, H. Yin and J. Yin, *Anal. Bioanal. Chem.*, 2020, **412**, 1915–1923.

25 N. Volpi, *Anal. Biochem.*, 2010, **397**, 12–23.

26 S. Tan, M. Johns and P. Greenfield, *Aust. J. Biotechnol.*, 1990, **4**, 38–43.

27 Q. Fan, Y. Gao, F. Mazur and R. Chandrawati, *Biomater. Sci.*, 2021, **9**, 6983–7007.

28 N. Shahbazi, R. Zare-Dorabei and S. M. Naghib, *Mater. Sci. Eng., C*, 2021, **127**, 112249.

29 R. D. Price, S. Myers, I. M. Leigh and H. A. Navsaria, *Am. J. Clin. Dermatol.*, 2005, **6**, 393–402.

30 R. S. Lamarca, N. da Costa Luchiari, A. F. Bonjorno, J. Passaretti Filho, A. A. Cardoso and P. C. F. de Lima Gomes, *Anal. Methods*, 2019, **11**, 3697–3705.

31 D. R. Albert, M. A. Todt and H. F. Davis, *J. Chem. Educ.*, 2012, **89**, 1432–1435.

32 T. S. Kuntzleman and E. C. Jacobson, *J. Chem. Educ.*, 2016, **93**, 1249–1252.

33 A. Saadati, F. Farshchi, M. Hasanzadeh and F. Seidi, *Anal. Methods*, 2021, **13**, 3909–3921.

34 M. M. Bordbar, A. Sheini, P. Hashemi, A. Hajian and H. Bagheri, *Biosensors*, 2021, **11**, 316.

35 S. Chandel and T. Agarwal, *Renewable Sustainable Energy Rev.*, 2017, **67**, 581–596.

36 T. Akyazi, L. Basabe-Desmonts and F. Benito-Lopez, *Anal. Chim. Acta*, 2018, **1001**, 1–17.

37 M. M. AlShehri and M. A. AlMeshal, *Arabian J. Chem.*, 2020, **13**, 2096–2100.

38 D. Mark, S. Haeberle, G. Roth, F. Von Stetten and R. Zengerle, *Microfluidics Based Microsystems: Fundamentals and Applications*, 2010, pp. 305–376.

39 G. de Carvalho Oliveira, C. C. S. Machado, D. K. Inácio, J. F. da Silveira Petruci and S. G. Silva, *Talanta*, 2022, **241**, 123244.

40 C. Zhang, J. Song, X. Shen, Q. Li, F. Su and S. Li, *J. Pharm. Biomed. Anal.*, 2023, **1**, 100001.

41 V. Malytskyi, J. Moreau, M. Callewaert, C. Henoumont, C. Cadiou, C. Feuillie, S. Laurent, M. Molinari and F. Chuburu, *Gels*, 2022, **8**, 182.

42 W. Wang, D. Li, Y. Zhang, W. Zhang, P. Ma, X. Wang, D. Song and Y. Sun, *Microchim. Acta*, 2020, **187**, 1–7.

43 J. Ge, R. Cai, L. Yang, L. Zhang, Y. Jiang, Y. Yang, C. Cui, S. Wan, X. Chu and W. Tan, *ACS Sustainable Chem. Eng.*, 2018, **6**, 16555–16562.

44 I. Skarmoutsos, A. Skarmoutsos, I. Katafigiotis, E. Tataki, A. Giagini, I. Adamakis, C. Alamanis, M. Duvdevani, N. Sitaras and C. Constantinides, *Med. Oncol.*, 2018, **35**, 1–6.

45 W. Yang, J. Ni, F. Luo, W. Weng, Q. Wei, Z. Lin and G. Chen, *Anal. Chem.*, 2017, **89**, 8384–8390.